Journal of Power Sources 207 (2012) 222–228

Contents lists available at SciVerse ScienceDirect

Journal of Power Sources

journal homepage: www.elsevier.com/locate/jpowsour

Controllable electrochemical synthesis and photovoltaic performance of ZnO/CdS core–shell nanorod arrays on fluorine-doped tin oxide

Chen-Zhong Yao*, Bo-Hui Wei, Li-Xin Meng, Hui Li, Qiao-Juan Gong, Hong Sun, Hui-Xuan Ma, Xiao-Hua Hu

Department of Applied Chemistry, Yuncheng University, Yuncheng 044000, China

ARTICLE INFO

Article history:
Received 12 October 2011
Received in revised form 30 January 2012
Accepted 31 January 2012
Available online 9 February 2012

Keywords:
Nanorod arrays
Semiconductor-sensitized solar cells
Electrodeposition

ABSTRACT

High density and vertical ZnO/CdS core–shell nanorod arrays have been prepared directly on FTO substrates via a two-step electrochemical deposition process. The length of ZnO nanorods and loading of CdS can be readily tuned by modulating the electrodeposition time, which influences on the photovoltaic performances of quantum dot-sensitized solar cells based on the ZnO/CdS core–shell nanorod arrays. The power conversion efficiency of the solar cell based on a ZnO nanorod array of 6.8 μm in length can achieve 1.07% with a J_{sc} of 5.42 mA cm^{-2} and a V_{oc} of 578 mV under 100 mW cm^{-2} of AM 1.5 G illumination.

1. Introduction

The exploitation of solar energy is of great interest for the environment pollution and energy crisis. Today, a number of photovoltaic devices have been developed for solar energy utilization [1,2]. Among these photovoltaic devices, dye-sensitized solar cells (DSSCs) and semiconductor-sensitized solar cells (SSSCs) are the promising candidates due to their unique size- and shapedependent absorption properties [3–5]. To enhance the power conversion efficiency of DSSCs or SSSCs, much attention has been paid to increasing light harvesting, accelerating electron transport and reducing charge recombination [6–10].

ZnO has been widely applied in solar cells, UV photodetectors, photocatalysis, field emission, light-emitting diodes, etc. [11–17]. ZnO nanorod arrays have been demonstrated great applications in DSSCs. They could provide a higher interfacial area and faster electrical pathways for the transport of electrons to increase the photo-electric conversion efficiency. However, due to its wide band gap (~3.37 eV), ZnO has a poor ability to absorb and utilize the visible light in solar cell applications, which can result in the low efficiency [18–22]. Surface modification of ZnO with narrow band-gap materials such as CdS, CdSe has been recognized as an efficient technique to improve the light-harvesting capacity of ZnO [23–27]. Recently, SSSCs based on CdS sensitized ZnO nanoarrays have been variously studied. Norris et al. reported 0.4% photovoltaic performance based on CdSe sensitized ZnO nanowire arrays (12 μm in length) [25]. Han et al. got a power conversion efficiency of 0.54% for CdS quantum dots (QDs) sensitized ZnO nanorod arrays [28]. Wang et al. also fabricated ZnO nanowires arrays/CdS QDs heterogeneous films and obtained a conversion efficiency of 0.34% [29]. However, the extremely long growth time and complicated process are necessary for the preparation of QDs sensitized ZnO nanoarrays in the above literatures. In addition, the efficient of the SSSCs based on CdS or CdSe sensitized ZnO nanoarrays is still very low (less than 0.6%). Thus, the development of a facile and quick method for the synthesis of CdS or CdSe sensitized ZnO nanoarrays for efficient photovoltaic performance is still a challenge.

Template-free electrodeposition, as a simple, low temperature, and economical method, has shown its potential for large-scale production and tailoring the architectures of nanomaterials. It is essential for the fabrication of nanodevices to assemble nanostructure with a uniform size in ordered arrays, since such an organisation combines the merits of patterned arrays and nanometer-sized materials [30]. Two-step electrodeposition is the most suitable method for preparing high-quality heterojunction solar cells, avoiding the unfavourable reactions that occur at elevated temperatures. The thickness of the core and the length of the shell can be well controlled by tuning the deposition time and current density [31,32].

In this study, we present that two-step electrochemical approach is suitable for fabrication of high density and ordered ZnO/CdS core–shell nanorod arrays on fluorine-doped tin oxide (FTO)-coated glass substrates. First, ZnO nanorod arrays could be grown vertically on FTO substrates via electrodeposition, and then CdS nanoparticles were directly deposited on the surface of ZnO nanorods via a successive electrodeposition process to form

* Corresponding author. Tel.: +86 359 2090394; fax: +86 359 2090378.
E-mail address: yaochzh1999@126.com (C.-Z. Yao).

0378-7753/$ – see front matter © 2012 Elsevier B.V. All rights reserved.
doi:10.1016/j.jpowsour.2012.01.154

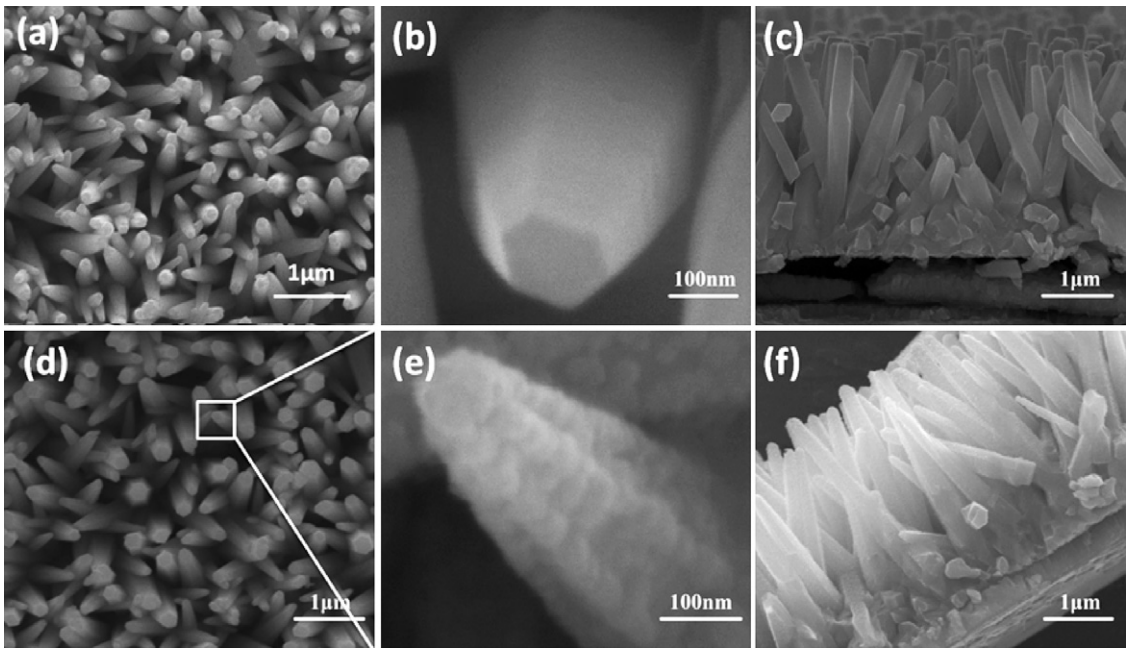

Fig. 1. Top-view and cross-sectional SEM images of (a–c) ZnO nanorod arrays synthesized on FTO substrates by galvanostatic electrolysis in aqueous solution of 0.02 M $Zn(NO_3)_2$, 0.01 M NH_4Ac, and 0.01 M $C_6H_{12}N_4$ (HMT) at 2.0 mA cm^{-2}, (d–f) ZnO/CdS core–shell nanorod arrays prepared by using the above ZnO nanorod arrays as working electrode in DMSO–H_2O (50 vol% DMSO:50 vol% H_2O) mixture solution containing 0.1 M $Cd(NO_3)_2$ and 0.1 M thiourea at 90 °C at 0.5 mA cm^{-2}.

the ZnO/CdS core–shell nanorod arrays. We further studied the influences of different electrodeposition time on the loading of CdS, length of ZnO nanorods, optical properties and photovoltaic performance of ZnO/CdS core–shell nanorod arrays were further investigated. The electrodeposited ZnO/CdS core–shell nanorod arrays can be used as photoanode for the solar cell application, exhibiting 1.07% power conversion efficiency under 100 mW cm^{-2} of AM 1.5 G illumination.

2. Experimental

2.1. Synthesis of ZnO nanorod arrays

All reagents were analytical grade and used directly without any purification. All the electrodeposition experiments were performed in a conventional three-electrode glass and the reaction temperature was controlled at 90 °C. During cathodic electrodeposition, a glass coated with F-doped SnO_2 (FTO) with a sheet resistance of 14 Ω $□^{-1}$ was used as the working electrode, a graphite rod of about 4.0 cm^2 was used as the auxiliary electrode, and a saturated Ag/AgCl electrode was used as the reference electrode. The FTO glass substrates were ultrasonically washed in deionized water, ethanol, and acetone for 30 min, respectively, and then rinsed in deionized water again before electrodeposition. ZnO nanorod arrays were synthesized on FTO substrates by galvanostatic electrolysis in aqueous solution of 0.02 M $Zn(NO_3)_2$, 0.01 M NH_4Ac, and 0.01 M $C_6H_{12}N_4$ (HMT) at 2.0 mA cm^{-2}. The length and diameter of ZnO nanorod can be controlled by changing the electrodeposition time. After the electrodeposition, the ZnO nanorod arrays on the FTO glass substrates was cleaned with deionized water and then used as the working electrode for the next electrodeposition.

2.2. Synthesis of ZnO/CdS core–shell nanorods

ZnO/CdS core–shell nanorod arrays were prepared via a electrodeposition process by using the above ZnO nanorod arrays as working electrode in DMSO–H_2O (50 vol% DMSO:50 vol% H_2O) mixture solutions, containing 0.1 M $Cd(NO_3)_2$ and 0.1 M thiourea at 90 °C. The deposition current density was 0.5 mA cm^{-2}. The loading of CdS on the ZnO nanorod surface can be tunable via the optimization of different electrodeposition time of CdS.

2.3. Characterizations

The samples (ZnO or ZnO/CdS nanorod arrays) were characterized by field emission scanning electron microscope (FE-SEM, JSM-6330F) with an energy dispersive spectroscopy (EDS, FEI/Quanta 400), X-Ray Diffractometer (XRD, D8 ADVANCE), transmission electron microscopy (TEM, JEM2010-HR). The optical properties of the ZnO nanostructures were measured with a UV–vis–NIR Spectrophotometer (UV, Shimadzu UV-3150). The current–voltage performance was measured using a Keithley 2400 source meter under simulated AM 1.5 G illumination (100 mW cm^{-2}) provided by solar simulator (69920, 1 kW Xe with optical filter, Oriel). The solar simulator was calibrated by a standard cell.

2.4. Device fabrication

To evaluate their photovoltaic performance, the CdS sensitized ZnO nanorods were sandwiched together with Pt coated fluorine-doped glass counter electrode, using front-side illumination conditions. Platinized counter electrodes were fabricated by thermal depositing H_2PtCl_6 onto the FTO coated glass. The mixture of 0.03 M I_2, 0.6 M 1-methyl-3-propylimidazolium iodide, 0.10 M guanidinium thiocyanate, and 0.5 M tertbutylpyridine in acetonitrile and valeronitrile (85:15), was introduced into the space between the sandwiched full cells.

3. Results and discussion

3.1. Morphology of ZnO/CdS core–shell nanorods

Fig. 1a–c is the typical SEM images of ZnO sample prepared by electrodeposition in aqueous solution containing 0.02 M $Zn(NO_3)_2$, 0.01 M NH_4Ac and 0.01 M HMT. The highly oriented ZnO nanorod arrays with smooth surface are uniformly covered onto the FTO

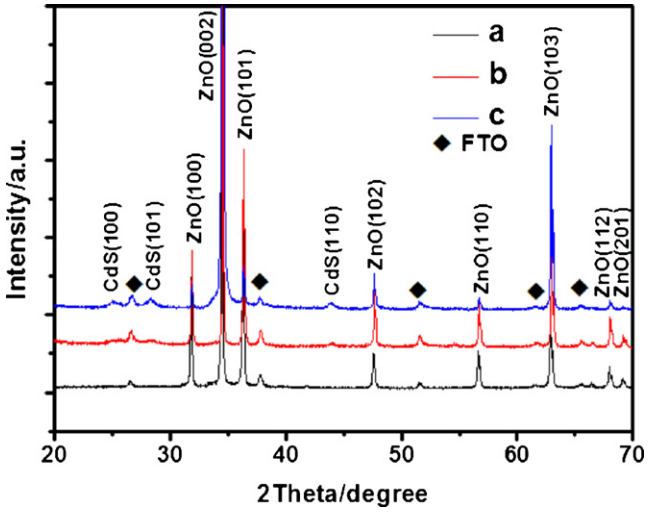

Fig. 2. XRD patterns of (a) ZnO nanorod arrays, (b) ZnO/CdS core–shell nanorod arrays, and (c) ZnO/CdS core–shell nanorod arrays annealed at 300 °C for 60 min in N_2 ambient.

glass substrates. The diameter and length of the ZnO nanorods are ~150 nm and ~2.5 μm, respectively. The as-prepared ZnO nanorod arrays/FTO glass were further electrodeposited at 90 °C in a DMSO–H_2O (50 vol% DMSO:50 vol% H_2O) mixture solution containing 0.1 M $Cd(NO_3)_2$ and 0.1 M thiourea for 10 min. The color of ZnO/FTO film changed from white to yellow, implying the formation of CdS on the ZnO surface. Fig. 1d–f is the SEM image of the ZnO/CdS sample after the electrodeposition of CdS, the morphology of nanorod remains constant. Moreover, the high-magnification SEM image (Fig. 1e) reveals the ZnO nanorods become rough covered with a number of small nanoparticles compared with the very smooth surface without CdS (Fig. 1b), implying the formation of CdS onto the ZnO nanorod surface. After heat treatment at 300 °C for 60 min in N_2 ambient, the morphology of ZnO/CdS core–shell nanorods is nearly as same as the as-prepared sample, and the corresponding SEM image is presented in Fig. S1.

3.2. Structure of ZnO/CdS core–shell nanorods

XRD measurement was carried out to study the crystal structure of the samples. Fig. 2a shows the typical XRD pattern of as-prepared ZnO, which can be indexed to a hexagonal wurtzite structure of ZnO (JCPDS: 36-1451) with lattice constants a = 3.25 Å and c = 5.207 Å. No other peaks besides SnO_2 peaks corresponding to the substrates (FTO glass) were detected, which suggests the sample is in good purity. The XRD pattern (Fig. 2, curve b) demonstrates that the CdS with a hexagonal structure (JCPDS: 65-3414, a = 4.132 Å, c = 6.734 Å) was successfully observed after a successive electrodeposition process in DMSO–H_2O mixture solution containing $Cd(NO_3)_2$ and thiourea. Furthermore, after calcination of ZnO/CdS/FTO sample (curve c and Fig. S2), the intensity of ZnO and CdS peaks was significantly stronger than those from curve b, indicating the crystallinity was improved via the calcination.

The detailed crystal structure and composition of the product were further characterized by TEM. Fig. 3 shows TEM images of as-electrodeposited ZnO/CdS core–shell nanorods. Clearly, the surface of the ZnO nanorods is uniformly coated with a number of CdS nanoparticles, as shown in Fig. 3a. The HRTEM and SAED results (inset in Fig. 3a and b) reveal that the ZnO nanorods are single crystalline with a [0 0 0 1] preferential growth direction and the CdS nanoparticles has a poor crystalline. The poor crystalline of CdS may influence on the properties and further applications. The as-prepared ZnO/CdS samples were calcined at 300 °C for 60 min in

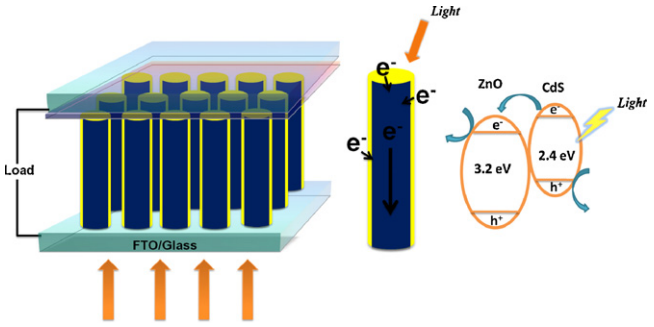

Scheme 1. Transfer of photo-generated electrons and holes in ZnO–CdS core–shell nanorod arrays under visible-light irradiation.

N_2 ambient in order to improve the crystalline quality. Fig. 4 is the TEM and HRTEM images of the ZnO/CdS core–shell nanorods after heat treatment. It clearly reveals the morphology keeps constant compared with the as-prepared samples (Fig. 3a). However, the SAED patterns of the calcined ZnO/CdS nanorod (Fig. 4b) display that a series of bright dots come from single crystal hexagonal ZnO and diffraction rings originated from the polycrystalline hexagonal CdS are clearly observed. Moreover, the HRTEM image (Fig. 4d) of ZnO/CdS core–shell interface region (marked by a white circle in Fig. 4c) shows a 0.31 nm CdS (1 0 1) lattice fringe spacing and a 0.52 nm ZnO (0 0 1) lattice fringe spacing, respectively. Hence, the HRTEM and SAED results disclose that the polycrystalline hexagonal CdS shells were grown on the surface of the hexagonal single crystalline ZnO nanorods and the crystallization of CdS shells can be obviously improved after a simple heat treatment. Fig. 4e–h presents the corresponding EDS elemental mapping of Cd, S, Zn, and O. It is found that Zn is densely distributed in the core area due to its smaller distribution, while Cd and S are spreading evenly around the surface of ZnO nanorods The atom ratio of Cd and S is about 1.07:1.This suggests the ZnO/CdS core–shell structures can be obtained via a two-step electrodeposition process.

3.3. Photovoltaic performance of ZnO/CdS nanorods

3.3.1. Photovoltaic performance dependence with ZnO/CdS annealing

It is known that the charge separation and electron accumulation in the metal–semiconductor and semiconductor–semiconductor junctions with suitable band gap position is much better than the single semiconductor [23,24]. Narrow band gap semiconductor CdS uniformly covered on the wide band gap materials ZnO nanorods are very attractive for the photovoltaic application. In our case, the ZnO and CdS can be formed a type-II band-gap alignment, as shown in Scheme 1. In this band-gap configuration, when electron–hole pairs are generated by light excitation in the conduction band of the CdS, the photoelectrons can be produced and transferred to the conduction band of the ZnO nanorods. This will greatly facilitate the charge separation process of electron–hole pairs before they recombine. Besides, the single-crystalline and highly ordered ZnO nanorods as core can provide a high accessible surface area for support CdS and shorten the conduction pathways for electrons to transport to the collection electrode, which will improve their photovoltaic performance. Fig. 5 shows the current–voltage curves of the solar cells based on the ZnO/CdS core–shell nanorod array films of the as-prepared and calcined under AM 1.5 G illumination at 100 mW cm^{-2}. It shows a short circuit photocurrent density (J_{sc}) of 2.92 mA cm^{-2}, an open circuit potential (V_{oc}) of 554 mV, a fill-factor (FF) of 0.312, and a power conversion efficiency (η) of 0.505% were obtained for the SSSCs based on the

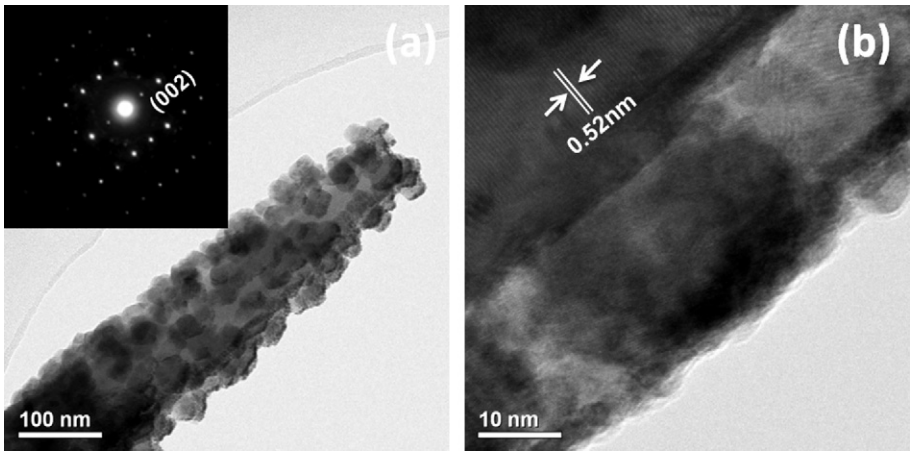

Fig. 3. (a) TEM image and (b) HRTEM images of calcined ZnO/CdS core–shell nanorods (inset is the corresponding SAED pattern).

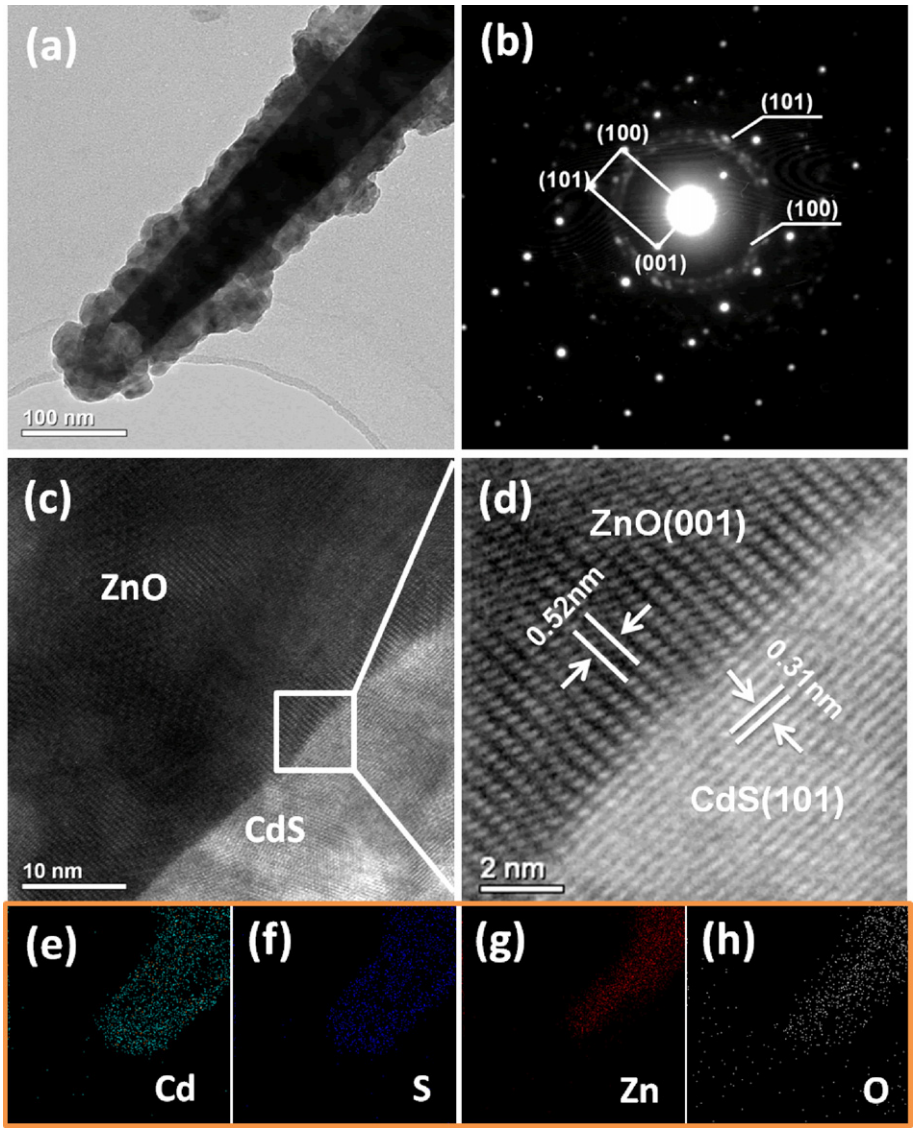

Fig. 4. (a) TEM image, (b) SAED pattern, (c and d) HRTEM images of ZnO/CdS core–shell nanorod annealed at 300 °C for 60 min in N_2 ambient. And the corresponding EDS elemental mapping images of (e) Cd, (f) S, (g) Zn and (h) O.

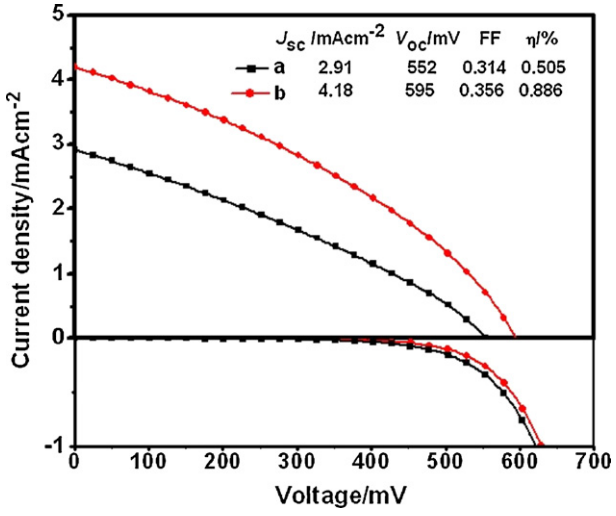

Fig. 5. Current–voltage curves of SSSCs based on as-prepared (curve a) or calcined (300 °C for 60 min in N_2 ambient, curve b) ZnO/CdS core–shell nanorod arrays under 100 mW cm^{-2} of AM 1.5 G illumination.

as-electrodeposited ZnO/CdS photoelectrode. Interestingly, the photovoltaic parameters (J_{sc}, V_{oc}, FF, η) of the SSSCs will increase to 4.18 mA cm^{-2}, 594 mV, 0.356, 0.886%, respectively, when the as-prepared ZnO/CdS photoelectrodes were annealed at 300 °C for 60 min in N_2 ambient. It shows the photocurrent, photovoltage, and fill factor increase significantly for the calcined ZnO/CdS solar cells. Compared with the as-prepared samples, the light absorption edge of the annealed sample shows no any change, as shown in Fig. S3. Thus, the great enhancement (from 0.505% to 0.886%) of photovoltaic performance is mainly ascribed to the improvement of crystallinity of ZnO/CdS. The dark current curves (Fig. 5) show the calcined ZnO/CdS core–shell films have a more negative onset potential than the as-prepared ZnO/CdS film, which might be resulted from an increase in an injection yield to ZnO due to the improved crystallinity of CdS.

3.3.2. *Photovoltaic performance dependence with CdS deposition time*

The influence of electrodeposited CdS on the photovoltaic performance of solar cells was further investigated. All the samples were annealed at 300 °C for 60 min in N_2 ambient before tested. The SEM images of ZnO/CdS core–shell nanorod arrays with CdS deposition times of 5–20 min are shown in Figs. S4–S6. It is found that more and more CdS nanoparticles were deposited on the surface of ZnO nanorods when increasing the CdS electrodeposition time. Fig. 6 shows the absorption spectra of the ZnO/CdS core–shell nanorod arrays with different CdS deposition times, which reveals the light absorption edge continuously shifts to longer wavelength with much longer CdS deposition time. This maybe attributed to the increases of CdS grain size with longer deposition process. A similar phenomenon has been reported [32,33].

The current–voltage curves of SSSCs based on the ZnO/CdS core–shell nanorod array films for different CdS deposition times are illustrated in Fig. 7. Detail photovoltaic performance parameters are also summarized in Table 1. As shown in Fig. 7 and Table 1, the J_{sc} varied from 2.38 mA cm^{-2}, 4.18 mA cm^{-2}, 3.91 mA cm^{-2} to 2.26 mA cm^{-2} when the electrodeposition time of CdS is changed from 5 min, 10 min, 15 min to 20 min, respectively. And the V_{oc} also shows a similar trend, namely, firstly increase and reach a maximum, and then decrease with the electrodeposition time. The optimized electrodeposition time may be attributed to the optical spacer effect and the good protection of active layer from CdS diffusion and charge extraction without introducing more series

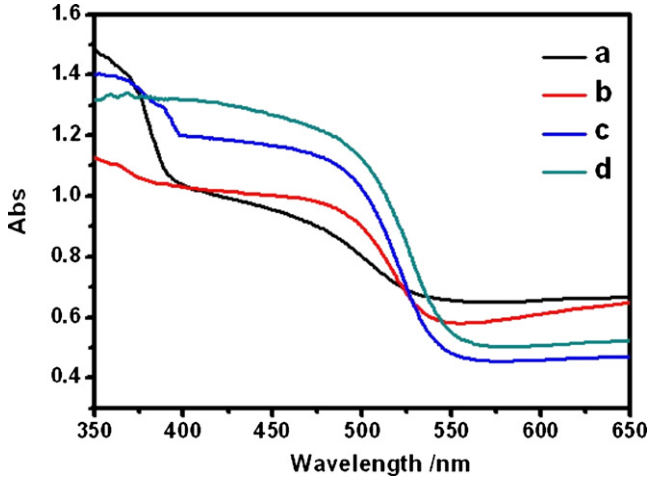

Fig. 6. UV–vis absorption spectra of ZnO/CdS core–shell nanorod arrays with different CdS deposition times (a) 5 min, (b) 10 min, (c) 15 min, and (d) 20 min.

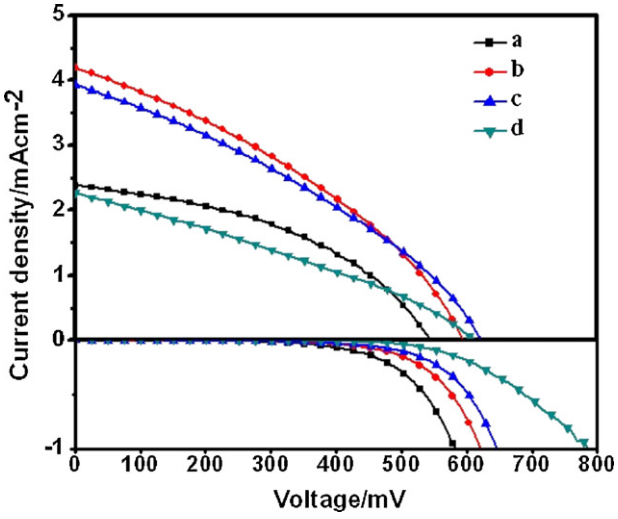

Fig. 7. Current–voltage curves of SSSCs based on ZnO/CdS core–shell nanorods with different CdS deposition times under 100 mW cm^{-2} of AM 1.5 G illumination. (a) 5 min, (b) 10 min, (c) 15 min, and (d) 20 min.

resistance. With a shorter electrodeposition time, the amount of CdS on the ZnO nanorod surface is smaller, and a less absorption of visible light is responsible for the lower photocurrent. Moreover, the electron recombination between ZnO and I_3^- in the electrolyte would be enhanced because of the direct exposure of ZnO in the electrolyte. It will result in the lower photovoltage and current. With the amount of CdS on the ZnO nanorod increases, the light absorption will increase, and the direct electron recombination between ZnO and electrolyte will be reduced, which can improve the photocurrent and voltage. However, the excess deposition of CdS on the ZnO nanorods surface would form a thick shell and act as a potential barrier for charge transfer, leading to lower power

Table 1
Detailed photovoltaic parameters of solar cells based on ZnO/CdS core–shell nanorods with different CdS deposition times under AM 1.5 G one sun illumination.

CdS deposition time (min)	J_{sc} (mA cm^{-2})	V_{oc} (mV)	FF	η (%)
5	2.38	543	0.432	0.559
10	4.18	595	0.356	0.886
15	3.91	618	0.343	0.829
20	2.26	608	0.314	0.431

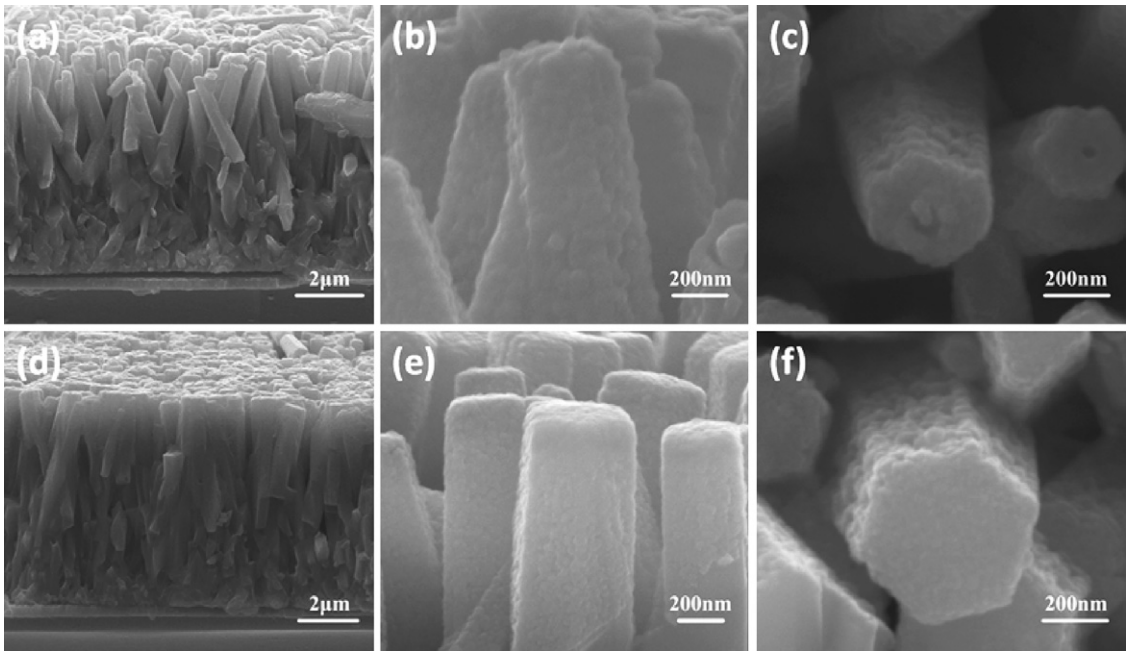

Fig. 8. SEM images of ZnO/CdS core–shell nanorod arrays prepared at different ZnO electrodeposition time (a–c) 90 min, and (d–f) 120 min of ZnO and with same electrodeposition time of CdS (10 min) after heat treatment at 300 °C for 60 min in N_2 ambient.

conversion efficiency [26,34]. The FF and dark current decrease with the increasing CdS deposition time as shown in Table 1. The decrease of FF is due to the internal resistance of solar cell gone up gradually with the increasing amount of CdS on the surface of ZnO nanorods. The thick shell formed by the excess deposition of CdS not only prevents photogenerated electron–hole pairs in the CdS nanoparticles from separating fast, but also restrains the recombination between electrons in the conduction band of ZnO and I_3^- in the electrolyte. Therefore, the optimum loading of CdS is crucial for the efficient photovoltaic performance of solar cells constructed with ZnO/CdS core–shell nanorod array films.

3.3.3. *Photovoltaic performance dependence with ZnO length and diameter*

The length and diameter of ZnO nanorods can be further controlled by tunable electrodeposition time, which was found to have an influence on the photovoltaic performance of SSSCs. Fig. 8 shows the SEM images of ZnO/CdS core–shell nanorod arrays prepared at different electrodeposition time (90 min or 120 min) of ZnO and with same electrodeposition time of CdS (10 min) after heat treatment at 300 °C for 60 min in N_2 ambient. After 90 min electrodeposition of ZnO, the length and diameter of ZnO/CdS nanorod arrays are 5.8 μm and 400 nm, respectively, shown in Fig. 8a–c. With a prolonged electrodeposition time of 120 min, the corresponding length and diameter of ZnO/CdS nanorod arrays increased to 6.8 μm and 500 nm (Fig. 8d–f), respectively. Clearly, both the length and the diameter of ZnO nanorods increase with the prolonged electrodeposition time from 50 min, 90 min to 120 min. This has been already observed for the synthesis of ZnO nanorod array previously [35,36]. It is known that the ZnO has a strong preferential orientation along the [0 0 0 1] direction, and ZnO nanorods are generally obtained when the [0 0 0 1] direction is not suppressed. In our case, the growth rate along [0 0 0 1] direction is faster than that of lateral growth during electrodeposition, resulting in the formation of nanorods. Furthermore, the length and diameter of the ZnO nanorods will increase due to the top and lateral of ZnO nanorods continuously grow with the prolonged electrodeposition time.

The effects of the length and diameter of ZnO nanorod arrays on the photovoltaic performance of CdS sensitized ZnO nanorod arrays films were further investigated. Fig. 9 displays the current–voltage curves of SSSCs based on ZnO/CdS core–shell nanorod array with different electrodeposition time of ZnO. With the prolongation of electrodeposition time of ZnO, namely the larger length and diameter of ZnO nanorods, the photocurrent increases from 4.18 mA cm^{-2}, 4.69 mA cm^{-2} to 5.42 mA cm^{-2}, and hence the power conversion efficiency of the solar cells are 0.88% for 50 min, 0.96% for 90 min and 1.07% for 120 min, respectively. To our knowledge, the photovoltaic performance (1.07%) of SSSCs based on the present ZnO/CdS core–shell nanorods made by a two-electrodeposition process is much higher than those of SSSCs based on CdS (∼0.54%) or CdSe (∼0.4%) sensitized ZnO nanorod arrays prepared via colloid method or successive ionic layer adsorption and reaction method [25,26,28,29]. Also, Lee et al. has reported that a higher power conversion efficiency of 1.5% can be achieved

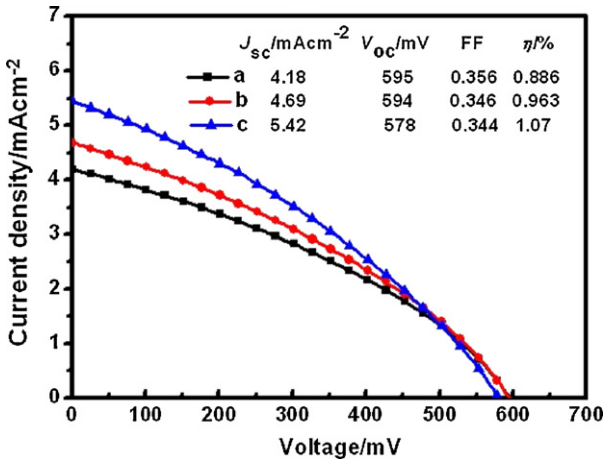

Fig. 9. Current–voltage curves of SSSCs based on ZnO/CdS core–shell nanorods prepared with different electrodeposition time of ZnO (keep constant CdS deposition time: 10 min) under 100 mW cm^{-2} of AM 1.5 G illumination. (a) 50 min, (b) 90 min, and (c) 120 min.

from the TiO_2@CdS solar cells by increasing surface area by growing vertically aligned NWs with high aspect ratio and high density [37]. Here, it is clear that the photovoltaic performance of SSSCs increase with the increasing length and diameter of ZnO nanorods, which have larger surface for the higher loading of CdS absorber. Generally, higher density ZnO nanorods pre unit areas, which have larger surface area, are more favorable for the enhancement of photovoltaic performance. Therefore, longer length and smaller diameter of ZnO nanorod are desired and could be expected to further enhance photovoltaic performance, which are under investigation.

4. Conclusion

In summary, vertical ZnO/CdS core–shell nanorod arrays were successfully synthesized on FTO glass substrates via a simple two-step electrochemical process. We have demonstrated the application of this core–shell structure as an efficient photoanode in quantum dot-sensitized solar cells, exhibiting a maximum power conversion efficiency of 1.07% with a J_{sc} of 5.42 mA cm^{-2} and a V_{oc} of 578 mV under AM 1.5 G (100 mW cm^{-2}) illumination. Further experiments show the photovoltaic performance of SSSCs strongly depends on the CdS deposition time and length of ZnO/CdS core–shell nanorods arrays. This work provides a facile electrochemical method to fabricate the desirable photoanodes with core–shell structure for efficient solar energy applications.

Acknowledgements

This work was supported by the Natural Science Foundations of China (Grant Nos. 20873184, 51101138 and 90923008), S & T project of Shanxi Province (Grant Nos. 20111024 and 20081044), and Young Teacher Starting-up Research of Yuncheng University (Grant Nos. YQ-2010013). We also thank X.H. Lu and B.X. Lei (Sun Yat-sen University) for the help of SSSCs measurements.

Appendix A. Supplementary data

SEM images of ZnO/CdS core–shell nanorod arrays with different CdS deposition times annealed at 300 °C for 60 min in N_2 ambient. Enlarged XRD patterns of (a) ZnO nanorod arrays, (b) ZnO/CdS core–shell nanorod arrays, and (c) ZnO/CdS core–shell nanorod arrays annealed at 300 °C for 60 min in N_2 ambient.

Supplementary data associated with this article can be found, in the online version, at doi:10.1016/j.jpowsour.2012.01.154.

References

[1] N.S. Lewis, G.W. Crabtree, A.J. Nozik, M.R. Wasielewski, A.P. Alivisatos, Office of Science, U.S. Department of Energy, April 18–21, 2005, Washington, DC, 2005.
[2] B.A. Gregg, J. Phys. Chem. B 107 (2003) 4688.
[3] B. O'Regan, M. Grätzel, Nature 353 (1991) 737.
[4] M.K. Nazeeruddin, F. De Angelis, S. Fantacci, A. Selloni, G. Viscardi, P. Liska, S. Ito, B. Takeru, M. Grätzel, J. Am. Chem. Soc. 127 (2005) 16835.
[5] P.V. Kamat, J. Phys. Chem. C 112 (2008) 18737.
[6] D. Kuang, J. Brillet, P. Chen, M. Takata, S. Uchida, H. Miura, K. Sumioka, S.M. Zakeeruddin, M. Grätzel, ACS Nano 2 (2008) 1113.
[7] A. Kongkanand, K. Tvrdy, K. Takechi, M. Kuno, P.V. Kamat, J. Am. Chem. Soc. 130 (2008) 4007.
[8] S. Anandan, Sol. Energy Mater. Sol. Cells 91 (2007) 843.
[9] D.B. Kuang, S. Uchida, R. Humphry-Baker, S.M. Zakeeruddin, M. Grätzel, Angew. Chem. Int. Ed. 47 (2008) 1923.
[10] M. Law, L.E. Greene, J.C. Johnson, R. Saykally, P.D. Yang, Nat. Mater. 4 (2005) 455.
[11] I. Gonzalez-Valls, Y.H. Yu, B. Ballesteros, J. Oro, M. Lira-Cantu, J. Power Sources 196 (2011) 6609.
[12] Q.F. Zhang, C.S. Dandeneau, X.Y. Zhou, G.Z. Cao, Adv. Mater. 21 (2009) 4087.
[13] N. Ye, J.J. Qi, Z. Qi, X.M. Zhang, Y. Yang, J. Liu, Y. Zhang, J. Power Sources 195 (2010) 5806.
[14] J.M. Bao, M.A. Zimmler, F. Capasso, X.W. Wang, Z.F. Ren, Nano Lett. 6 (2006) 1719.
[15] F. Lu, W.P. Cai, Y.G. Zhang, Adv. Funct. Mater. 18 (2008) 1047.
[16] X.H. Lu, D. Wang, G.R. Li, C.Y. Su, D.B. Kuang, Y.X. Tong, J. Phys. Chem. C 113 (2009) 13574.
[17] J.C. She, Z.M. Xiao, Y.H. Yang, S.Z. Deng, J. Chen, G.W. Yang, N.S. Xu, ACS Nano 2 (2008) 2015.
[18] M. Guo, P. Diao, X.D. Wang, S.M. Cai, J. Solid State Chem. 178 (2005) 3210.
[19] J.B. Baxter, A.M. Walker, K. van. Ommering, E.S. Aydil, Nanotechnology 17 (2006) S304.
[20] A.B. Martinson, J.W. Elam, J.T. Hupp, M.J. Pellin, Nano Lett. 7 (2007) 2183.
[21] Y.F. Gao, M. Nagai, Langmuir 22 (2006) 3936.
[22] I. Gonzalez-Valls, M. Lira-Cantu, Energy Environ. Sci. 2 (2009) 19.
[23] G. Liu, Z.G. Chen, F. Li, L.Z. Wang, G.Q. Lu, Chem. Commun. (2009) 3452.
[24] Y. Tak, S.J. Hong, J.S. Lee, K.J. Yong, J. Mater. Chem. 19 (2009) 5945.
[25] K.S. Leschkies, R. Divakar, J. Basu, E. Enache-Pommer, J.E. Boercker, C.B. Carter, U.R. Kortshagen, D.J. Norris, S.A. Aydil, Nano Lett. 7 (2007) 1793.
[26] Y.W. Tang, X.Y. Hua, M.J. Chen, L.J. Luo, B.H. Li, L.Z. Zhang, Electrochim. Acta 54 (2009) 2742.
[27] F. Fang, D.X. Zhao, B.H. Li, Z.Z. Zhang, J.Y. Zhang, D.Z. Shen, Appl. Phys. Lett. 93 (2008) 233115.
[28] W. Lee, S.K. Min, V. Dhas, S.B. Ogale, S.H. Han, Electrochem. Commun. 11 (2008) 103.
[29] Y. Zhang, T. Xie, T. Jiang, X. Wei, S. Pang, X. Wang, D.J. Wang, Nanotechnology 20 (2009) 155707.
[30] J. Elias, C. Levy-Clement, M. Bechelany, J. Michler, G.Y. Wang, Z. Wang, L. Philippe, Adv. Mater. 22 (2010) 1607.
[31] J. Katayama, K. Ito, M. Matsuoka, J. Tamaki, J. Appl. Electrochem. 34 (2004) 687.
[32] J.B. Cui, U.J. Gibson, J. Phys. Chem. C 114 (2010) 6408.
[33] C.H. Chang, Y.L. Lee, Appl. Phys. Lett. 91 (2007) 053503.
[34] H.M. Jia, H. Xu, Y. Hu, Y.W. Tang, L.J. Zhang, Electrochem. Commun. 9 (2007) 354.
[35] S.K. Park, J.H. Park, K.Y. Ko, S. Yoon, K.S. Chu, W. Kim, Y.R. Do, Cryst. Growth Des. 9 (2009) 3615.
[36] J. Elias, R. Tena-Zaera, C. Lévy-clément, J. Electroanal. Chem. 621 (2008) 171.
[37] J.C. Lee, T.G. Kim, W. Lee, S.H. Han, Y.M. Sung, Cryst. Growth Des. 9 (2009) 4519.